MSDE

COMMUNICATION

View Article Online
View Journal | View Issue

Cite this: *Mol. Syst. Des. Eng.*, 2022, 7, 1415

Received 1st September 2022,
Accepted 4th October 2022

DOI: 10.1039/d2me00185c

rsc.li/molecular-engineering

A 2,7-dichlorofluorescein derivative to monitor microcalcifications†

Patrik Tholen,‡[b] Connor N. Brown,‡[a] Claudia Keil,[b] Ali Bayir,[c] Hui-Hui Zeng,[d] Hajo Haase,[b] Richard B. Thompson,[d] Imre Lengyel[a] and Gündoğ Yücesan §*[b]

Herein, we report the crystal structure of 2,7-dichlorofluorescein methyl ester (DCF-ME) and its fluorescence response to hydroxyapatite binding. The reported fluorophore is very selective for staining the bone matrix and provides turn-on fluorescence upon hydroxyapatite binding. The reported fluorophore can readily pass the cell membrane of the C2C12 cell line, and it is non-toxic for the cell line. The reported fluorophore DCF-ME may find applications in monitoring bone remodeling and microcalcification as an early diagnosis tool for breast cancer and age-related macular degeneration.

Design, System, Application

Microcalcification is an integral part of pathologies in breast cancer, pseudoxanthoma elasticum (PXE), age-related macular degeneration (AMD), and Alzheimer's disease (AD), among others. The number of fluorescent probes described to selectively detect microcalcifications to elucidate and potentially diagnose above mentioned diseases, and bone remodeling is very limited in the literature. In this work, we report the design and synthesis of a new fluorescent probe DCF-ME, which is highly selective for staining microcalcifications and bone. Furthermore, the novel structure of DCF-ME generates synergistic interactions between the bound microcalcifications, calcium ions and the fluorescent core. Upon hydroxyapatite binding, DCF-ME exhibits a 2.5-fold increase in fluorescence intensity, which is confirmed by lifetime measurements. DCF-ME was found to be non-toxic for the C2C12 cell line and it readily passes C2C12 cell membrane. DCF-ME provides an excellent platform for a new class of turn-on fluorescence probe for monitoring microcalcifications for early diagnosis, like that in cancer, macular degeneration or rare diseases like PXE, or monitoring bone remodeling for osteoporosis treatments.

Calcium is an essential metal ion in biology.[1] Calcium ions take part in signal transduction as a messenger and are essential for muscle contraction.[2] In addition, calcium, together with phosphates, comprise hydroxyapatite (HAP) to form the mineral part of bone structure.[3] Moreover, microcalcification is an integral part of pathologies in breast cancer, pseudoxanthoma elasticum (PXE), age-related macular degeneration (AMD), and Alzheimer's disease (AD), among others.[4] Macrocalcifications can be detected by computerized tomography, but this cannot resolve small mineral particles,[5] although microcalcification could be an early sign of the development of disease.[6] Fluorescence imaging technologies could help to monitor the development and growth of these seed calcifications and thus potentially become a diagnostic tool for diseases in which microcalcifications play a role. Small molecule fluorescent probes that exhibit high affinity and selective binding to HAP can help identify such deposits; these probes are distinct from the well-known fluorescent probes that recognize free ionic calcium.[7]

However, the number of fluorescent probes specific for hydroxyapatite or calcium-rich minerals is limited in the literature. Previously, Frangioni has used bisphosphonate-functionalized cyanine fluorophores to monitor bone remodeling. These compounds are costly due to the multiple-step syntheses and have issues with toxicity limiting their applications in human subjects.[8] Another HAP-specific fluorophore, which has a monobisphosphonate attached to the fluorescein core *via* an aliphatic side chain, was also proven to be HAP sensitive.[9] Such fluorophores only carry the

[a] *Wellcome-Wolfson Institute for Experimental Medicine, Queen's University Belfast, Belfast BT9 7BL, UK*
[b] *Institute for Food Chemistry and Toxicology, Germany, Technische Universität Berlin, Gustav-Meyer-Allee 25, 13355 Berlin, Germany.*
E-mail: yuecesan@tu-berlin.de, guendog.yuecesan@hhu.de
[c] *The Department of Chemistry, Yıldız Technical University, 34220, Esenler, Istanbul, Turkey*
[d] *Department of Biochemistry and Molecular Biology, University of Maryland School of Medicine, Baltimore, Maryland 21201, USA*

† Electronic supplementary information (ESI) available: Experimental procedures and data, including XRD, bone staining images, and fluorescence spectra. Crystal structure data has been deposited to the Cambridge Crystal Structure Database with CCDC number 2203101. For ESI and crystallographic data in CIF or other electronic format see DOI: https://doi.org/10.1039/d2me00185c

‡ C. N. B. and P. T. have equally contributed to this work.

§ G. Y.'s current address is Institute of Inorganic and Structural Chemistry, Heinrich-Heine University, Düsseldorf, 40225, Germany.

fluorescent label to the target HAP site without providing a change in fluorescence upon binding. Alizarin S and von Kossa stains are colorimetric methods. Alizarin S binds to Ca minerals while von Kossa uses silver ions binding to phosphate.[10] We have also previously reported that phenylphosphonic acid tethered porphyrins could provide a turn-on response with increased fluorescence upon hydroxyapatite binding.[11] Here we explore the synthesis and use of 2,7-dichlorofluorescein methyl ester (DCF-ME) for labeling HAP mineralization. 2,7-Dichlorofluorescein (DCF) has two chelating sites that have a metal binding environment similar to those of 2,2′-bipyridine, 1,10-phenantroline, ortho-idimines or 1,2-benzoquinone. The chelating site of DCF-ME includes a chlorine atom at positions 2 and 7, and hydroxyl oxygen atoms at positions 3 and 6 of the fluorescein core. Despite the favorable chelating orientation of oxygen and chlorine atoms, 2,7-dichlorofluorescein derivatives haven't been used to target metal ions due to the weak affinity of chlorocarbon compounds for metal ions. While several main group chlorobenzene complexes have been described,[12] as well as coordination of cesium and thallium on 1,2-dicholorethane,[13,14] and silver complexes of dichloromethane and ethane,[13] chlorocarbon coordination hasn't been studied widely in the literature. Hypothetically, the relatively higher affinity of an adjacent oxygen atom could help the coordination of calcium atoms to the chlorine atoms as well in the case of DCF-ME (see Fig. 1A and B). To the best of our knowledge, naked 2,7-dichlorofluorescein derivatives have not been studied as ligands for hydroxyapatite.

Furthermore, coordination of a metal ion to fluorescein hydroxyl groups can generate direct synergistic interaction with the conjugated fluorescein core, which has been exploited for zinc sensors in the case of Zinpyr by Lippard.[15] In this study, we used another derivative of 2,7-dichlorofluorescein namely 2,7-dichlorofluorescein methyl ester (DCF-ME). We introduced the methyl group to the carboxyl group of fluorescein so that the stronger metal carboxylate coordination is eliminated in favor of oxygen and chlorine atoms. DCF-ME was previously described in a few reports as an ammonia[16] and hydrogen peroxide sensor,[17] but hasn't been used to target metal ions before. We also report here the crystal structure of DCF-ME for the first time in the literature.

Direct calcium coordination of the DCF-ME ring oxygens would likely create synergistic interactions between the calcium and the conjugated fluorescein core and might result in an increase or decrease in fluorescence upon calcium coordination to the sp^2 conjugated fluorescent core. In addition to Lippard's work,[15] we have recently reported a similar mechanism where we extended the conjugation of the fluorescent core *via* sp^2-bound phosphonates to calcium and other transition metal ions, generating alterations in fluorescence behaviour.[11,18]

In this work, we used a different structural strategy of altering the fluorescein structure to extend the conjugation of fluorescein without the help of ligands directing the metal coordination on the fluorescein hydroxyl group. The crystals of DCF-ME were obtained from a concentrated solution of water under normal conditions by slowly evaporating the solvent. The crystal structure was solved using SHELXT[19] and refined using SHELXL[20] in the Olex[2] software package[21] (see ESI† for crystal structure refinement information).

As shown in Fig. 1C, the crystal structure of DCF-ME is composed of one-dimensional hydrogen-bonded chains of DCF-ME. In the crystal structure, methyl ester oxygens are structurally hindered by the methyl groups and are not involved in hydrogen bond making. The hydrogen bonds between the fluorescein groups have distances of 2,57 and 2,67 Å, indicative of very strong near covalent hydrogen bond interactions.

After purification, the absorbance, emission, and excitation spectral characteristics of DCF-ME were determined in solutions of either phosphate-buffered saline (PBS), Tris-buffered saline (TBS), HEPES-saline (HEPES) and unbuffered saline solution (all made to 12 μM), aqueous buffers widely used in biological experiments. DCF-ME has a peak absorbance of 502 nm when diluted in TBS (Fig. 2A). No variation in maximal peak intensity and position was observed when comparing the absorbance of DCF-ME in PBS, TBS, HEPES or saline solution (Fig. S1†). There was minimal deterioration in the fluorescence intensity of the dye when stored at room temperature in any solution (with water replacing saline) over 14 days, indicating that the dye is relatively stable when diluted in these solvents (data not shown).

Upon binding of the fluorescent probe to CHTTM ceramic hydroxyapatite (CerHAP), there is an approximately 2.5-fold increase in the fluorescence intensities in all diluents (Fig. 2B), with no noticeable shift in the emission spectrum (Table S2†). This consistent increase in fluorescence intensity is substantially diminished when the beads were washed once in their respective buffers. The removal of excess and unbound dye led to a decrease in fluorescence intensity,

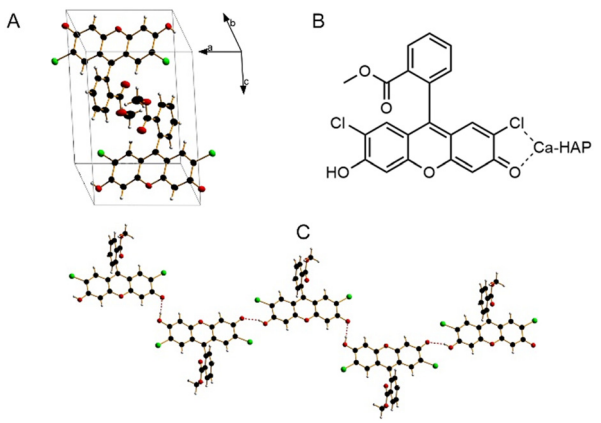

Fig. 1 Crystal structure of DCF-ME in a unit cell (A), potential Ca-HAP coordination modes (B) and one-dimensional hydrogen bonding pattern (C).

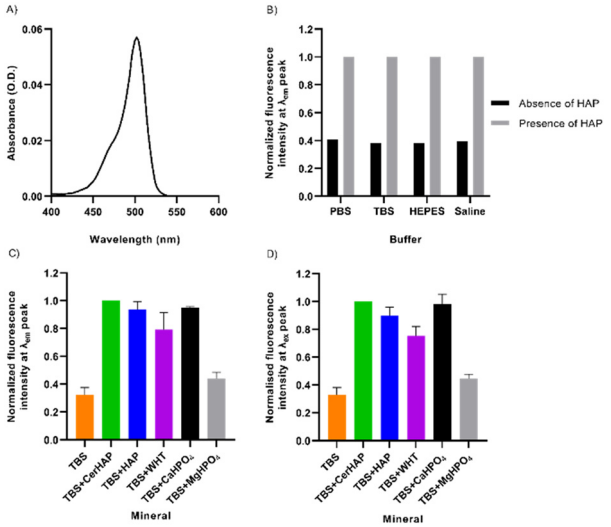

Fig. 2 Fluorescence characteristics of 12 μM DCF-ME in the absence and presence of various calcium phosphate minerals. A) The absorbance spectrum of DCF-ME in TBS. B) Normalized fluorescence intensity of DCF-ME, excited at λ_{ex} 460 nm, when diluted in different buffers, the presence and absence of CerHAP. C) Normalized fluorescence intensity of the mean peak emission of DCF-ME in TBS when incubated with various calcium phosphate minerals, excited at λ_{ex} 460 nm. D) Normalized fluorescence intensity of the mean corrected peak excitation of DCF-ME in TBS when incubated with various calcium phosphate minerals, using λ_{em} 570 nm. Data in A, C and D represent mean values, whilst C and D are ± S.D. (n = 3); for these experiments emission was measured with excitation at shorter wavelength (460 nm) than peak absorbance, and excitation with emission at longer wavelength (570 nm) than peak emission to minimize the effects of Rayleigh scattering.

leaving approximately 6.4–7.3% of dye remaining bound to the HAP beads (Table S2†). This is reflected in the spectra obtained when the dye was excited at 460 nm, giving an emission spectrum ranging between approximately 500–590 nm, with peak emission at 522–524 nm (Fig. S3†). The corrected excitation spectrum of 12 μM DCF-ME, remaining bound to HAP, ranges between 450–525 nm, with a peak excitation of 502 nm (Fig. S4†). The corrected excitation spectra for DCF-ME were obtained using a quantum counter to determine a correction factor calculated by measuring the absorbance and excitation spectra of Rhodamine 6G (1.25 μM in ethanol), measured at 600 nm.

The fluorescence characteristics of DCF-ME were further probed for its binding to different minerals (Fig. 2C). These included: synthetic HAP and whitlockite (WHT) (courtesy of Professor KT Nam),[22] dibasic calcium phosphate ($CaHPO_4$) and magnesium phosphate dibasic trihydrate ($MgHPO_4$), which were used as controls. At its peak emission, DCF-ME shows a 3.10-fold increase when bound to ceramic HAP, which is similar in each of the various diluents (Fig. 2B). When normalized to the values in the presence of ceramic HAP, both HAP and $CaHPO_4$ nanocrystals show similar fluorescence intensities, whilst binding to WHT led to lower fluorescence and binding to $MgHPO_4$ has a 2.26-fold decrease in fluorescence (Fig. 2C). This is also reflected in the corrected maximal excitation intensity of DCF-ME when bound to the various minerals, where there is a 3.05-fold increase in the intensity when bound to ceramic HAP (Fig. 2D). Again, when comparing the additional minerals to ceramic HAP, both mineral HAP and $CaHPO_4$ have similar excitation intensities (1.11-fold and 1.02-fold changes, respectively), whilst WHT shows a 1.33-fold change and $MgHPO_4$ shows a 2.25-fold change. The respective emission and excitation spectra for the DCF-ME (Fig. S5 and S6,† respectively) intensity remaining bound to the minerals show that there is no shift in the spectral properties of the dye and that the dye remains bound to the calcium–phosphate minerals more than WHT or $MgHPO_4$.

Since accurate measurement of fluorescence intensity changes in translucent mineral phases can be challenging, we also chose to confirm quantum yield increases by measuring changes in the fluorescence lifetime of DCF-ME upon binding to HAP in less polar solvents. We found (ESI,† Fig. S9) that there was a significant increase in amplitude-weighted average lifetime from two component fits in these frequency domain data sets from 4.21 ns in solution to 5.72 ns for the HAP-bound form in DMSO, clearly confirming the increases in quantum yield described above. Moreover, we observed small shifts in the DCF-ME excitation and emission spectra upon binding to HAP from DMSO (ESI† Fig. S10) that were unexpected since, among fluorophores, fluorescein derivatives are notably solvent-insensitive. Instead, these shifts provide supporting evidence for direct interaction for the fluorescein moiety with the HAP mineral, perhaps like that diagrammed in Fig. 1.

To assess the binding of DCF-ME to HAP in tissue, formalin-fixed, paraffin-embedded mouse rib sections were used. To determine the ability of the dye to label rib calcifications, we incubated sections with 1.2 mM, 120 μM and 12 μM DCF-ME in TBS and found no appreciable fluorescent signal at 12 μM with imaging settings established above this concentration (Fig. 3A–C, respectively). In further experiments, we used 120 μM DCF-ME to determine the time of incubation required to produce a fluorescence signal. Images were obtained after 120, 60, 30, 20, or 10 minute incubation times (Fig. 4A–E, respectively). A reliable fluorescence signal was achieved after a 30 minute incubation (Fig. 4). Tissue autofluorescence observed in the negative control (Fig. 4F) was lower than the DCF-ME-stained rib, making it distinguishable from DCF-ME fluorescence. To

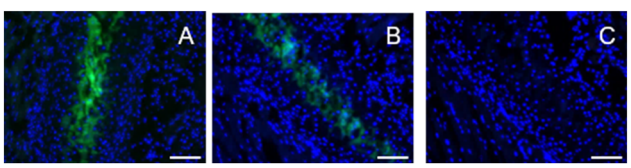

Fig. 3 Cancellous mouse ribs incubated with 1.2 mM (A), 120 μM (B) and 12 μM (C) DCF-ME ($\lambda_{ex/em}$ 480/527 nm; exposure time – 135 ms), diluted in TBS and counterstained with DAPI ($\lambda_{ex/em}$ 360/470 nm; exposure time – 50 ms). Scale bar = 100 μm.

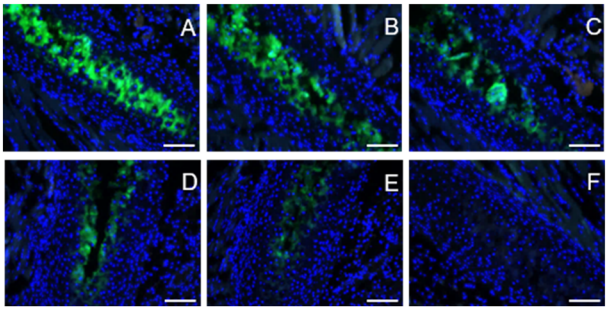

Fig. 4 Cancellous mouse ribs were incubated with 120 μM DCF-ME ($\lambda_{ex/em}$ 480/527 nm; exposure time – 135 ms), diluted in TBS, and counterstained with DAPI ($\lambda_{ex/em}$ 360/470 nm; exposure time – 50 ms). Incubation times of DCF-ME varied between 120, 60, 30, 20 and 10 min (A–E, respectively). Negative control of mouse ribs incubated with TBS alone is also included (F). Scale bar = 100 μm.

determine the binding of DCF-ME to rib in different buffers used in biological experiments, 120 μM DCF-ME was prepared in TBS, PBS, HEPES and saline (ESI† Fig. S6a–d, respectively). No difference in fluorescent signal was observed, and these signals remained essentially unchanged when intensities were imaged 4, 7 or 14 days after labeling showing that the binding to HAP is stable within this period (Fig. S7†).

To determine the cytocompatibility of DCF-ME, we transformed mouse C2C12 cells[23] into osteoblasts by exposing them to 500 ng mL^{-1} BMP-2 (recombinant human bone morphogenetic protein-2).[24] Differentiation was assessed by measuring alkaline phosphatase (ALP) activity after six days of incubation (Fig. 5A).[25] At this time point, osteoblasts do not produce microcalcifications yet.[26] To assess whether DCF-ME leads to cytotoxicity, the osteoblasts were exposed to different concentrations of DCF-ME, and cell viability was assessed *via* a MTT metabolic activity assay.[27]

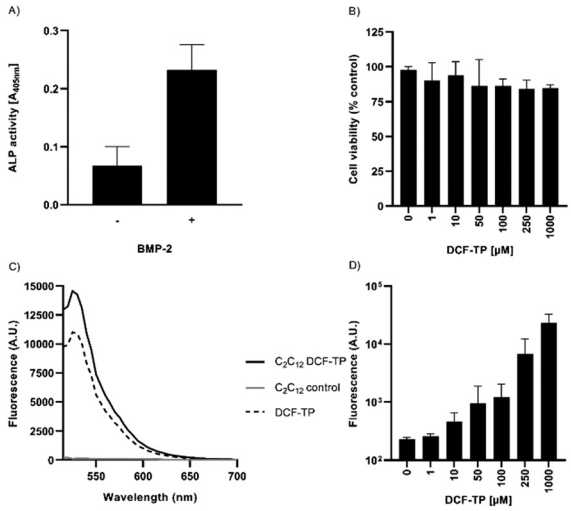

Fig. 5 Cell culture cytotoxicity in differentiated osteoblast cells, which were differentiated with BMP-2. A) ALP activity of C2C12 cells, with and without the addition of BMP-2 for 6 days. B) Cell viability following 24 h DCF-ME treatment was measured by a tetrazolium-based metabolic activity assay. Triton X-100 (0.5%) was used as a positive control, causing around 95.5% cytotoxicity (not shown). C) Fluorescence spectra of DCF-ME-exposed C2C12 cells in comparison to 10 μM DCF-ME dissolved in incubation buffer, using λ_{ex} 492 nm. D) Dose-dependency of cellular DCF-ME labeling ($\lambda_{ex/em}$ 492/530 nm). Data represent mean values ± S.D. from n = 3 independent experiments.

Increasing concentrations of DCF-ME had no statistically significant effect on cell viability to up to 1000 μM DCF-ME when compared to untreated controls (Fig. 5B). When differentiated C2C12 cells were incubated with DCF-ME and imaged under a fluorescence microscope, using an excitation of 488 nm and emission of 530 nm, we found a cell-associated increase in fluorescence intensity (Fig. 5C and S8†). This cell-associated fluorescent signal showed an increase in intensity with increasing concentrations of DCF-ME, up to 100 μM, with a larger increase in fluorescence intensity at 250 μM and 1000 μM DCF-ME (Fig. 5D).

Conclusions

In summary, we report the design and one-step synthesis of a new fluorescent probe for monitoring calcification termed DCF-ME. Unlike its 2,7-dichlorofluorescein core, the additional methyl group at the carboxylic acid tails of DCF made the fluorescein oxygen and chlorine atoms more available for calcium binding. We hypothesize that direct extension of fluorescein conjugation to the calcium atoms generated synergistic interactions. DCF-ME selectively stained the mineral portion of the bone which may be osteoblast-associated to some extent. Binding to HAP produces a strong increase in fluorescence intensity, confirmed by lifetime measurements, making DCF-ME a promising turn-on fluorescence probe for monitoring microcalcifications in some circumstances.

Should DCF-ME be considered for *in vivo* tomographic imaging, knowledge of cellular toxicity is a prerequisite. Within this study, osteogenic C2C12 cells were used to evaluate DCF-ME toxicity.[24] BMP-2 differentiated C2C12 cells, elevated in the osteoblast marker enzyme alkaline phosphatase (Fig. 5A), were unaffected in cellular metabolic activity upon treatment with DCF-ME up to concentrations far above those that would be used experimentally (1000 uM) (Fig. 5B). The fluorescence spectroscopic and microscopic data suggest that DCF-ME might be accessible to osteoblasts (Fig. 5C, D and S8†), similar to what has been previously observed for fluorescein-labelled risedronates in bone cells and tissues.[28] While the growth-inhibiting effect of some (bis)phosphonates is quite desirable for pharmacological treatment of a variety of bone tissue disorders,[29] covalent phosphonate attachment to rather moderately cytotoxic fluorescein seems to be a promising strategy to create cell-tolerable imaging agents for applications in bone biology and biomedicine.[30] Further *in vivo* toxicology is required to examine skeletal cellular specificity and the kinetics of distribution within bones and soft tissue organs to decide the possibility of future use in diagnostic assessments for

mineralization in humans. Moreover, DCF-ME may provide a new turn-on fluorescence probe for monitoring microcalcifications for early diagnoses, like cancer, macular degeneration, or rare diseases like PXE, or monitoring bone remodeling for osteoporosis treatments.

Author contributions

The manuscript was written through the contributions of all authors. All authors have approved the final version of the manuscript.

Conflicts of interest

R. B. T. is a principal of Pokegama Technologies, Inc.; no conflict declared.

Acknowledgements

G. Y. would like to thank the DFG for funding his work. C. N. B. would like to thank the Department for Education of Northern Ireland for his PhD studentship. I. L. would like to thank the Belfast Association for the Blind for supporting his research. R. B. T. and H.-H. Z. thank the U.S. National Eye Institute RO1 EY 030443 for their support. The authors thank Professor Ki Tae Nam (Department of Materials Science and Engineering, Seoul National University, Seoul, 151-744, South Korea; E-mail: nkitae@snu.ac.kr) for the generous gift of synthetic HAP and WHT nanocrystals.

References

1 W. Choi, N. Clemente, W. Sun, J. Du and W. Lü, The structures and gating mechanism of human calcium homeostasis modulator 2, *Nature*, 2019, **576**(7785), 163–167, DOI: **10.1038/s41586-019-1781-3**.

2 R. E. Dolmetsch, R. S. Lewis, C. C. Goodnow and J. I. Healy, Differential activation of transcription factors induced by Ca2+ response amplitude and duration, *Nature*, 1997, **386**(6627), 855–858, DOI: **10.1038/386855a0**; C.-H. Cho, J. S. Woo, C. F. Perez and E. H. Lee, A focus on extracellular Ca2+ entry into skeletal muscle, *Exp. Mol. Med.*, 2017, **49**(9), e378, DOI: **10.1038/emm.2017.208**; D. E. Clapham, Calcium Signaling, *Cell*, 2007, **131**(6), 1047–1058, DOI: **10.1016/j.cell.2007.11.028**.

3 A. S. Posner and F. Betts, Synthetic amorphous calcium phosphate and its relation to bone mineral structure, *Acc. Chem. Res.*, 1975, **8**(8), 273–281, DOI: **10.1021/ar50092a003**; A. Lotsari, A. K. Rajasekharan, M. Halvarsson and M. Andersson, Transformation of amorphous calcium phosphate to bone-like apatite, *Nat. Commun.*, 2018, **9**(1), 4170, DOI: **10.1038/s41467-018-06570-x**.

4 L. Omarjee, C. Roy, C. Leboeuf, J. Favre, D. Henrion, G. Mahe, G. Leftheriotis, L. Martin, A. Janin and G. Kauffenstein, Evidence of Cardiovascular Calcification and Fibrosis in Pseudoxanthoma Elasticum Mouse Models Subjected to DOCA-Salt Hypertension, *Sci. Rep.*, 2019, **9**(1), 16327, DOI: **10.1038/s41598-019-52808-z**; U. Dreses-Werringloer, J. C. Lambert, V. Vingtdeux, H. Zhao, H. Vais, A. Siebert, A. Jain, J. Koppel, A. Rovelet-Lecrux and D. Hannequin, *et al.*, A polymorphism in CALHM1 influences Ca2+ homeostasis, Abeta levels, and Alzheimer's disease risk, *Cell*, 2008, **133**(7), 1149–1161, DOI: **10.1016/j.cell.2008.05.048**; M. Alsheh Ali, K. Czene, P. Hall and K. Humphreys, Association of Microcalcification Clusters with Short-term Invasive Breast Cancer Risk and Breast Cancer Risk Factors, *Sci. Rep.*, 2019, **9**(1), 14604, DOI: **10.1038/s41598-019-51186-w**; A. Rizwan, S. K. Paidi, C. Zheng, M. Cheng, I. Barman and K. Glunde, Mapping the genetic basis of breast microcalcifications and their role in metastasis, *Sci. Rep.*, 2018, **8**(1), 11067, DOI: **10.1038/s41598-018-29330-9**; R. F. Cox, A. Hernandez-Santana, S. Ramdass, G. McMahon, J. H. Harmey and M. P. Morgan, Microcalcifications in breast cancer: novel insights into the molecular mechanism and functional consequence of mammary mineralisation, *Br. J. Cancer*, 2012, **106**(3), 525–537, DOI: **10.1038/bjc.2011.583**.

5 R. M. Rangayyan, F. J. Ayres and J. E. L. Desautels, A review of computer-aided diagnosis of breast cancer: Toward the detection of subtle signs, *J. Franklin Inst.*, 2007, **344**(3), 312–348, DOI: **10.1016/j.jfranklin.2006.09.003**; Z. Wang, N. Hauser, G. Singer, M. Trippel, R. A. Kubik-Huch, C. W. Schneider and M. Stampanoni, Non-invasive classification of microcalcifications with phase-contrast X-ray mammography, *Nat. Commun.*, 2014, **5**(1), 3797, DOI: **10.1038/ncomms4797**.

6 A. C. S. Tan, M. G. Pilgrim, S. Fearn, S. Bertazzo, E. Tsolaki, A. P. Morrell, M. Li, J. D. Messinger, R. Dolz-Marco and J. Lei, *et al.*, Calcified nodules in retinal drusen are associated with disease progression in age-related macular degeneration, *Sci. Transl. Med.*, 2018, **10**(466), eaat4544, DOI: **10.1126/scitranslmed.aat4544**; A. A. Bergen, S. Arya, C. Koster, M. G. Pilgrim, D. Wiatrek-Moumoulidis, P. J. van der Spek, S. M. Hauck, C. J. F. Boon, E. Emri and A. J. Stewart, *et al.*, On the origin of proteins in human drusen: The meet, greet and stick hypothesis, *Prog. Retinal Eye Res.*, 2019, **70**, 55–84, DOI: **10.1016/j.preteyeres.2018.12.003**; M. P. Morgan, M. M. Cooke and G. M. McCarthy, Microcalcifications Associated with Breast Cancer: An Epiphenomenon or Biologically Significant Feature of Selected Tumors?, *J. Mammary Gland Biol. Neoplasia*, 2005, **10**(2), 181–187, DOI: **10.1007/s10911-005-5400-6**.

7 G. Grynkiewicz, M. Poenie and R. Y. Tsien, A new generation of Ca2+ indicators with greatly improved fluorescence properties, *J. Biol. Chem.*, 1985, **260**(6), 3440–3450, DOI: **10.1016/S0021-9258(19)83641-4**.

8 H. Hyun, H. Wada, K. Bao, J. Gravier, Y. Yadav, M. Laramie, M. Henary, J. V. Frangioni and H. S. Choi, Phosphonated near-infrared fluorophores for biomedical imaging of bone, *Angew. Chem., Int. Ed.*, 2014, **53**(40), 10668–10672, DOI: **10.1002/anie.201404930**; K. R. Bhushan, E. Tanaka and J. V. Frangioni, Synthesis of Conjugatable Bisphosphonates for Molecular Imaging of Large Animals, *Angew. Chem., Int. Ed.*, 2007, **46**(42), 7969–7971, DOI: **10.1002/anie.200701216**.

9 A. M. Sim, N. A. Rashdan, L. Cui, A. J. Moss, F. Nudelman, M. R. Dweck, V. E. MacRae and A. N. Hulme,

A novel fluorescein-bisphosphonate based diagnostic tool for the detection of hydroxyapatite in both cell and tissue models, *Sci. Rep.*, 2018, **8**(1), 17360, DOI: **10.1038/s41598-018-35454-9**.

10 H. Puchtler, S. N. Meloan and M. S. Terry, On the history and mechanism of alizarin and alizarin red s stains for calcium, *J. Histochem. Cytochem.*, 1969, **17**(2), 110–124, DOI: **10.1177/17.2.110**; S. N. Meloan and H. Puchtler, Chemical Mechanisms of Staining Methods: Von Kossa's Technique: What von Kossa Really Wrote and a Modified Reaction for Selective Demonstration of Inorganic Phosphates, *J. Histotechnol.*, 1985, **8**(1), 11–13, DOI: **10.1179/his.1985.8.1.11**.

11 Y. Zorlu, C. Brown, C. Keil, M. M. Ayhan, H. Haase, R. B. Thompson, I. Lengyel and G. Yücesan, Fluorescent Arylphosphonic Acids: Synergic Interactions between Bone and the Fluorescent Core, *Chemistry*, 2020, **26**(49), 11129–11134, DOI: **10.1002/chem.202001613**.

12 A. V. Korolev, F. Delpech, S. Dagorne, I. A. Guzei and R. F. Jordan, Main-Group-Metal Chlorobenzene Complexes, *Organometallics*, 2001, **20**(16), 3367–3369, DOI: **10.1021/om010395a**.

13 M. R. Colsman, T. D. Newbound, L. J. Marshall, M. D. Noirot, M. M. Miller, G. P. Wulfsberg, J. S. Frye, O. P. Anderson and S. H. Strauss, Silver(I) complexes of dichloromethane and 1,2-dichloroethane, *J. Am. Chem. Soc.*, 1990, **112**(6), 2349–2362, DOI: **10.1021/ja00162a040**.

14 T. G. Levitskaia, J. C. Bryan, R. A. Sachleben, J. D. Lamb and B. A. Moyer, Bidentate coordination of 1,2-dichloroethane to Cs+ was reported recently, *J. Am. Chem. Soc.*, 2000, **122**, 554.

15 X. A. Zhang, D. Hayes, S. J. Smith, S. Friedle and S. J. Lippard, New strategy for quantifying biological zinc by a modified zinpyr fluorescence sensor, *J. Am. Chem. Soc.*, 2008, **130**, 15788; G. K. Walkup, S. C. Burdette, S. J. Lippard and R. Y. Tsien, A New Cell-Permeable Fluorescent Probe for Zn2+, *J. Am. Chem. Soc.*, 2000, **122**(23), 5644–5645, DOI: **10.1021/ja000868p**.

16 K. Waich, T. Mayr and I. Klimant, Fluorescence sensors for trace monitoring of dissolved ammonia, *Talanta*, 2008, **77**(1), 66–72, DOI: **10.1016/j.talanta.2008.05.058**.

17 S. M. Borisov, T. Mayr, G. Mistlberger, K. Waich, K. Koren, P. Chojnacki and I. Klimant, Precipitation as a simple and versatile method for preparation of optical nanochemosensors, *Talanta*, 2009, **79**(5), 1322–1330, DOI: **10.1016/j.talanta.2009.05.041**.

18 C. Keil, J. Klein, F.-J. Schmitt, Y. Zorlu, H. Haase and G. Yücesan, Arylphosphonate-Tethered Porphyrins: Fluorescence Silencing Speaks a Metal Language in Living Enterocytes, *ChemBioChem*, 2021, **22**(11), 1925–1931, DOI: **10.1002/cbic.202100031**.

19 G. M. Sheldrick, SHELXT-Integrated Space-Group andCrystal-Structure Determination, *Acta Crystallogr., Sect. A: Found. Adv.*, 2015, **71**, 3.

20 G. Sheldrick, A short history of SHELX, *Acta Crystallogr., Sect. A: Found. Crystallogr.*, 2008, **64**(Pt 1), 12–22, DOI: **10.1107/S0108767307043930**; G. M. Sheldrick, *Program for the Refinement of Crystal Structures from Diffraction Data, SHELXL-93*, 1993.

21 O. V. Dolomanov, L. Bourhis, R. J. Gildea, J. A. K. Howard and H. Puschmann, OLEX2: A Complete Structure Solution, Refinement and Analysis Program, *J. Appl. Crystallogr.*, 2009, **42**, 339.

22 H. L. Jang, G. B. Zheng, J. Park, H. D. Kim, H.-R. Baek, H. K. Lee, K. Lee, H. N. Han, C.-K. Lee, N. S. Hwang, J. H. Lee and K. T. Nam, *et al.*, In Vitro and In Vivo Evaluation of Whitlockite Biocompatibility: Comparative Study with Hydroxyapatite and β-Tricalcium Phosphate, *Adv. Healthcare Mater.*, 2016, **5**(1), 128–136, DOI: **10.1002/adhm.201400824**.

23 D. Yaffe and O. R. A. Saxel, Serial passaging and differentiation of myogenic cells isolated from dystrophic mouse muscle, *Nature*, 1977, **270**(5639), 725–727, DOI: **10.1038/270725a0**.

24 T. Katagiri, A. Yamaguchi, M. Komaki, E. Abe, N. Takahashi, T. Ikeda, V. Rosen, J. M. Wozney, A. Fujisawa-Sehara and T. Suda, Bone morphogenetic protein-2 converts the differentiation pathway of C2C12 myoblasts into the osteoblast lineage, *J. Cell Biol.*, 1994, **127**(6), 1755–1766, DOI: **10.1083/jcb.127.6.1755**.

25 E. Heining, R. Bhushan, P. Paarmann, Y. I. Henis and P. Knaus, Spatial Segregation of BMP/Smad Signaling Affects Osteoblast Differentiation in C2C12 Cells, *PLoS One*, 2011, **6**(10), e25163, DOI: **10.1371/journal.pone.0025163**.

26 R. Song, D. Wang, R. Zeng and J. Wang, Synergistic effects of fibroblast growth factor-2 and bone morphogenetic protein-2 on bone induction, *Mol. Med. Rep.*, 2017, **16**(4), 4483–4492, DOI: **10.3892/mmr.2017.7183**.

27 M. Maares, A. Duman, C. Keil, T. Schwerdtle and H. Haase, The impact of apical and basolateral albumin on intestinal zinc resorption in the Caco-2/HT-29-MTX co-culture model†, *Metallomics*, 2018, **10**(7), 979–991, DOI: **10.1039/c8mt00064f**.

28 A. J. Roelofs, F. P. Coxon, F. H. Ebetino, M. W. Lundy, Z. J. Henneman, G. H. Nancollas, S. Sun, K. M. Blazewska, J. L. F. Bala and B. A. Kashemirov, *et al.*, Fluorescent risedronate analogues reveal bisphosphonate uptake by bone marrow monocytes and localization around osteocytes in vivo, *J. Bone Miner. Res.*, 2010, **25**(3), 606–616, DOI: **10.1359/jbmr.091009**; J. A. F. Vermeer, I. D. C. Jansen, M. Marthi, F. P. Coxon, C. E. McKenna, S. Sun, T. J. de Vries and V. Everts, Jaw bone marrow-derived osteoclast precursors internalize more bisphosphonate than long-bone marrow precursors, *Bone*, 2013, **57**(1), 242–251, DOI: **10.1016/j.bone.2013.08.007**.

29 K. B. Farrell, A. Karpeisky, D. H. Thamm and S. Zinnen, Bisphosphonate conjugation for bone specific drug targeting, *Bone Rep.*, 2018, **9**, 47–60, DOI: **10.1016/j.bonr.2018.06.007**; M. Pazianas, S. van der Geest and P. Miller, Bisphosphonates and bone quality, *BoneKEy Rep.*, 2014, **3**, 529, DOI: **10.1038/bonekey.2014.24**; R. G. G. Russell,

M. J. Rogers, J. C. Frith, S. P. Luckman, F. P. Coxon, H. L. Benford, P. I. Croucher, C. Shipman and H. A. Fleisch, The pharmacology of bisphosphonates and new insights into their mechanisms of action, *J. Bone Miner. Res.*, 1999, **14**(S2), 53–65, DOI: **10.1002/jbmr.5650140212**.

30 R. Alford, H. M. Simpson, J. Duberman, G. C. Hill, M. Ogawa, C. Regino, H. Kobayashi and P. L. Choyke, Toxicity of Organic Fluorophores Used in Molecular Imaging: Literature Review, *Mol. Imaging*, 2009, **8**(6), 7290.2009.00031, DOI: **10.2310/7290.2009.00031**.